

Magnetic and structural enhanced characterization of Zr-Al substituted M-type barium hexaferrite

H. A. Shahia^a, M. S. Shifa^b, M. M. Alam^b, H. M. N. U. H. K. Asghar^c,
Z. A. Gilani^{c,*}, S. M. Ali^d, M. Z. Nawaz^e, M. A. Sharf^f, A. A. Alhazaa^d, A. K.
Khan^g

^aDepartment of Physics, Govt College University Faisalabad, Allama Iqbal Road, Faisalabad, Pakistan

^bInstitute of Physics, The Islamia University of Bahawalpur, Bahawalpur, 63100, Pakistan

^cDepartment of Physics, Balochistan University of Information Technology, Engineering & Management Sciences, Quetta 87300, Pakistan

^dDepartment of Physics and Astronomy, College of Science, P.O. BOX 2455, King Saud University, Riyadh, 11451, Saudi Arabia

^eDepartment of Materials Science and Engineering, Southern University of Science and Technology, Shenzhen 518055, China

^fDepartment of Mechanical & Energy Systems Engineering, Faculty of Engineering and Informatics, University of Bradford, Bradford BD7 1DP, United Kingdom

^gDepartment of Physics, University of Central Punjab, Bahawalpur Campus, Bahawalpur, Pakistan

Co-precipitation method was used to fabricate Zr-Al substituted M-Type barium hexagonal ferrite with a unique composition $Ba_{1-x}Zr_{0.5x}Al_{0.3}Fe_{11.7}O_{19}$ ($x = 0.0, 0.1, 0.2, 0.3, 0.4,$ and 0.5). The materials were characterized using Fourier Transform Infrared spectroscopy and a magnetic hysteresis loop. For each sample, the values of M_s , H_c , M_r , remanence ratios (M_r/M_s), and magneton number (nB) are determined using M-H loops. The M_r/M_s ratio of the synthesized hexaferrites particles is between 0.001017 and 0.143103, indicating a single magnetic domain. FTIR spectroscopy was used to study the inter-atomic forces and gives information about the absorption and emission spectrum for solids, liquids and gases. The results indicate that the synthesized compounds may have potential use as perpendicular magnetic recording media due to the growing trend in saturation magnetization, remanence, and coercivity.

(Received April 4, 2024; Accepted July 4, 2024)

Keywords: Zr-Al, Barium, Hexagonal ferrites, Co-precipitation, FTIR, VSM

1. Introduction

Nano particles are commonly utilized in current technologies and everyday goods. Atoms or molecules joined together and smaller than 100 nm are known as nanoparticles. Ferrites are oxide-based ceramic compositions in which iron is the predominant element. Ferrites are soft and hard magnetic materials. They have a tremendously magnetic character. Spinel ferrites, Garnets, Ortho ferrites, and hexaferrites are the four types of ferrites. Hard ferrites are only hexagonal; all others are soft.

The chemical stability, low cost, and wide range of technological applications of ferrites based on magnate make them the most important materials. These include ferrofluids, high-quality filters, transformer cores, magnetic recording media, biomedical fields, and medical diagnostics[1]. Due to their crystal structure, hexagonal ferrites are able to be magnetized easily

* Corresponding authors: zagilani2002@yahoo.com
<https://doi.org/10.15251/JOR.2024.204.445>

along the c axis and exhibit high levels of uniaxial magnetocrystalline anisotropy. Most replacements in hexagonal ferrites reduce the anisotropy field, which produces hysteresis properties that are advantageous in many settings[2]. As a result of their high coercivity, remanence, magnetic energy product, and uniaxial magnetocrystalline anisotropy, as well as their excellent oxidation resistance, hexagonal ferrites (chemical formula: $MFe_{12}O_{19}$) find wide applicability as permanent magnets, microwave devices, magneto-optics, and magnetic recording media[3].

We used hard ferrites in our investigation. A permanent magnet, recording medium, supercapacitor component, acoustic device, magnetic hose (to transmit magnetic field due to ferromagnetic nature), microwave electronic device, and many more uses are all part of the extensive list of uses for M-type hexaferrite $AFe_{12}O_{19}$ (A= Ba, Sr, Pb)[4]. Hexagonal ferrites are useful for applications involving radar and high frequency absorption due to their improved magnetic characteristics. The unit cell of M-Type hexaferrites has lattice parameters of $a=5.88\text{\AA}$ and $c=23.2\text{\AA}$. With a magnetic moment of $5\ \mu_B$, M-type barium hexaferrites ($BaFe_{12}O_{19}$) exhibit a magnetic character as Fe^{+3} ions. This is the subject of our research.

The M-Type barium hexaferrites are often prepared using the high energy ball milling method [5], the sol-gel method [6], the Co-precipitation technique[7], hydro thermal treatment, chemical mixing , etc. The co-precipitation process is the most efficient, simple, low-cost, and manageable way to get hexaferrites material. We want to learn more about M-Type barium hexaferrites that have been co-precipitated and replaced with Zr-Al (with $x = 0.0, 0.1, 0.2, 0.3, 0.4, 0.5$) and have the formula $Ba_{1-x}Zr_{0.5x}Al_{0.3}Fe_{11.7}O_{19}$. High-frequency and static magnetic characteristics have been determined.

2. Experimental procedure

$Ba_{1-x}Zr_{0.5x}Al_{0.3}Fe_{11.7}O_{19}$ hexaferrites with $x=0.0, 0.1, 0.2, 0.3, 0.4,$ and 0.5 was prepared by Co-precipitation method which was reported iRASD (Journal of Materials and Physical Sciences) [8]. VSM was used to study the magnetic property of the materials. The M-type hexaferrites' structural phase was determined using FTIR (Fourier transformation infrared analysis).

2.1. M- H loop or magnetic properties

The M-Type hexagonal ferrites $Ba_{1-x}Zr_{0.5x}Al_{0.3}Fe_{11.7}O_{19}$ ($x = 0.0, 0.1, 0.2, 0.3, 0.4, 0.5$) magnetic hysteresis loops are shown in Figure 1.1. For each sample, the values of M_s , H_c , M_r , remanence ratios or squareness ratios (M_r/M_s), and magneton number (n_B) are determined using M-H hysteresis loops, as indicated in table 1.1. In Figure 1.1 we see how the magnets' saturation magnetization (M_s) and coercivity (H_c) change as the Zr concentration changes. The distribution of cations, porosity, chemical composition, and grain size all affect the pattern and width of (M-H) loops[9]. The hysteresis loop is generated using a vibrating sample magnetometer (VSM). The phenomenon of super exchange contact is linked to magnetization, which is caused by the movement of iron (Fe) ions at five crystallographic sites, including 2a-2b-12k (spin up) and 4f1 and 4f2 (spin down)[10].

An equation describing the relationship between magnetization (M) and high magnetic fields (H) is given below[11].

$$M = M_s \left(1 - \frac{A}{H} - \frac{B}{H^2} \right) + \chi_p H \quad (1)$$

The external magnetic field is denoted by H, inhomogeneity constant by A, and susceptibility by X. Constant A is close to zero and is neglected in a high magnetic field. Therefore, equation (1) is simplified into the following equation (2)[12]

$$M = M_s \left(1 - \frac{B}{H^2} \right) \quad (2)$$

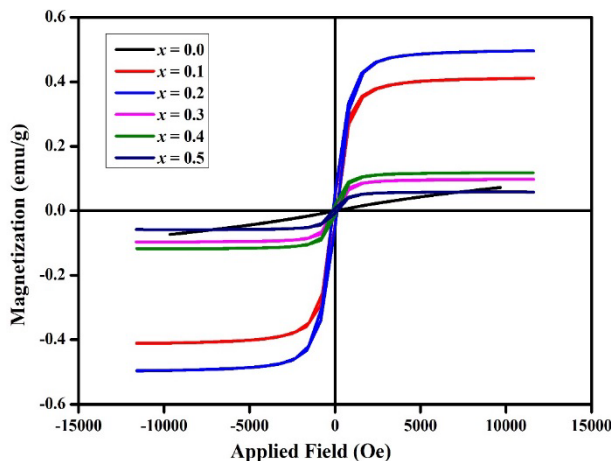


Fig. 1. Magnetic hysteresis loop for M-type hexaferrites $Ba_{1-x}Zr_{0.5x}Al_{0.3}Fe_{11.7}O_{19}$ ($x = 0.0, 0.1, 0.2, 0.3, 0.4, 0.5$).

The prepared materials possess low coercivity H_c as shown in the M-H loop and it is the property of the soft ferrites. Fe^{3+} has a high spin, while Fe^{2+} has a low spin. The M_r and M_s ranges from (0.00000118-0.051) and (0.07-0.496) respectively. The Zr content may be varied to find the minimal value of M_s at $x = 0.0$, as shown in Figure 2(a, b). Afterwards, it shows an upward trend until $x = 0.2$, after which it declines. In the hexagonal ferrite unit cell, different cationic locations are linked to different M_s values. The declining trend in M_s is related to the magnetic moment of the non-magnetic replacement ion. Substitution of hexaferrites with non-magnetic large-sized ions often occurs at octahedral sites such as $12k$, $2a$, and $4f_2$ [13].

Furthermore, collinear arrangement of magnetically momentous Fe^{3+} ions is a result of the existence of super exchange contact. Changes in M_s may be directly traced to shifts in the distributions of cations at the surface's spin effect and A/B sites. With M_b and M_a standing for the relative magnetizations at sites B and A, respectively, the total magnetization is given by $M_{total} = M_b - M_a$ [14]. As the Zr concentrations increased up to $x = 0.2$, the increase in magnetism may be due to the A-site replacement. Ions of iron show ferromagnetic behavior, while ions of zirconium are paramagnetic by nature. As the concentration of Zr^{4+} ions increase, the electronic spin at the Fe^{3+} site changes from collinear to non-collinear. Reductions in M_s and magnetic moment are brought about by the shifting behavior of electronic spin[15].

The higher ionic radii of substituted ions compared to Fe^{3+} ions are another factor that causes H_c decrease. With a lower M_r at increased substitution, the synthesized material may be used for high-speed recording. Recording media applications need low coercivity ferrite with high saturation magnetization. Therefore, Zr replacement has the benefit of producing excellent recording qualities while only employing small amounts of dopants [2]. The hysteresis loop has been used to determine magnetic parameters, and these parameters have been used to calculate the squareness ratio (M_r/M_s). When this value is at or above 0.5, the material is in a single magnetic domain; when it is below 0.5, multi-domain structures may be forming[16]. According to this study, the material exhibits a multi-domain structure with a squareness ratio ranging from 0.001017 to 0.156364.

Table 1. M-type hexaferrites' saturation magnetization (M_s), remanence (M_r), coercivity (H_c), and squareness ratio (M_r/M_s) for each composition of $Ba_{1-x}Zr_{0.5x}Al_{0.3}Fe_{11.7}O_{19}$ ($x = 0.0, 0.1, 0.2, 0.3, 0.4, 0.5$).

X	Sat. Mag M_s (emu/g)	H_c (Oe)	Remnant Mag. M_r (emu/g)	Squareness ratio M_r/M_s	Molecular Mass	Magnetic Moment nB (μB)
0	0.07	0.00000118	0.0000712	0.001017	1102.788	0.01382
0.1	0.411	0.0051	0.04	0.097324	1093.62	0.080479
0.2	0.496	0.000267	0.051	0.102823	1084.445	0.096309
0.3	0.097	0.00000149	0.0137	0.141237	1075.274	0.018675
0.4	0.11	0.000031	0.0172	0.156364	1055.102	0.020998
0.5	0.58	0.0000179	0.0083	0.143103	1056.93	0.010976

Using Eq (3), the connection between Ms and a number of magnetons nB was computed.

$$\text{Magnetons number } (n_B) = \frac{MM_s}{5585} \quad (3)$$

In this case, Ms is the total molecular mass and M is the magnetization of the whole composition[17]. According to Table 1, the addition of Zr^{4+} raises the Bohr magneton number by an amount between 0.010976 μ_B and 0.096309 μ_B . The saturation magnetization trend was detected for nB because it is a function of Ms and M.W (molecular weight) of the sample [18]. The microstructure of MPs determines both their intrinsic and extrinsic behaviors, including the Hc, which is related to the cation distribution, size, and shape of the crystal.

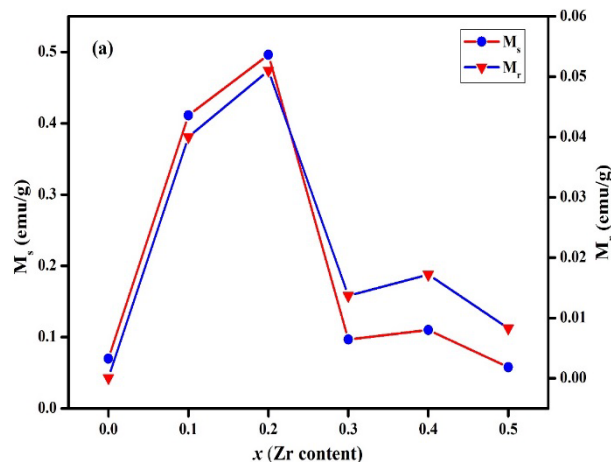


Fig. 2. Influence of Zr concentration (x) on saturation and remnant magnetization of the M-Type $Ba_{1-x}Zr_{0.5x}Al_{0.3}Fe_{11.7}O_{19}$ ($x = 0.0, 0.1, 0.2, 0.3, 0.4, 0.5$) hexaferrites.

The magnetic single as well as the multi-domain nature of samples may be determined by the squareness ratio. In general, ferrites with a squareness ratio more than 0.5 are single-domain materials, whereas those with a squareness ratio less than 0.5 are multi-domain materials[18-21]. These ferrites' squareness ratio values fell between 0.001017 and 0.156364, according to the research. As a result, the ferrites are all multi-domain materials. Multiple domains were likely responsible for the samples' weak coercivity[22].

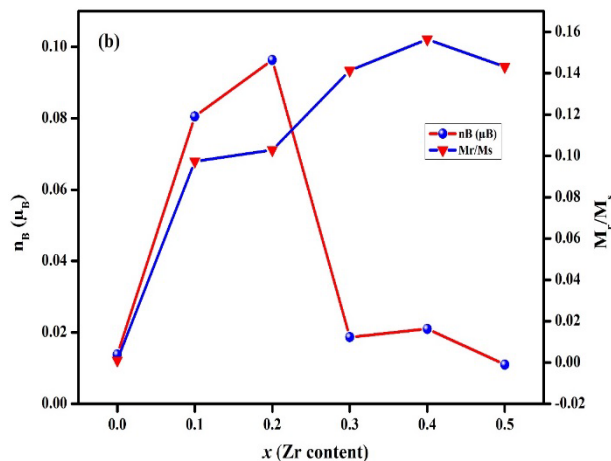


Fig. 3. Influence of Zr concentration (x) on nB and Mr/Ms of the M-Type $Ba_{1-x}Zr_{0.5x}Al_{0.3}Fe_{11.7}O_{19}$ ($x = 0.0, 0.1, 0.2, 0.3, 0.4, 0.5$) hexaferrites.

2.2. FTIR analysis

To study the inter atomic forces caused due to the atomic vibration we use Fourier Transmission Infrared spectroscopy. It is also gives the absorption and emission spectrum for solids, liquids and gases. We can guess the purity of the materials by using the FTIR analysis. Figures 4(a,b,c,d,e,f) show the FTIR spectra of every sample of $Ba_{1-x}Zr_{0.5x}Al_{0.3}Fe_{11.7}O_{19}$ ($x = 0.0, 0.1, 0.2, 0.3, 0.4, \text{ and } 0.5$), with a wave number range of 400 cm^{-1} to 4000 cm^{-1} .

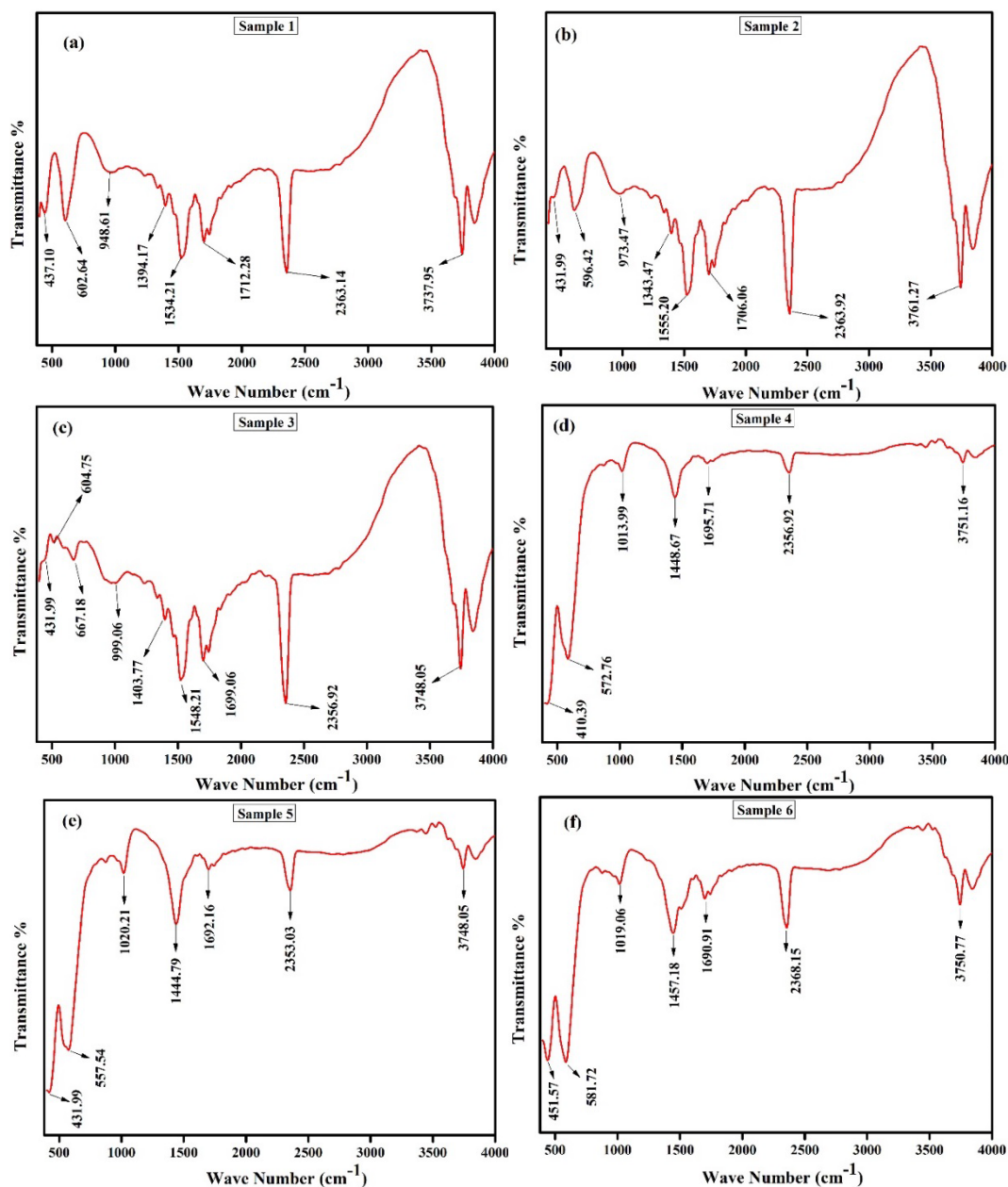


Fig. 4. (a, b, c, d, e, f) Shows the spectra of FTIR for M-type hexaferrites $Ba_{1-x}Zr_{0.5x}Al_{0.3}Fe_{11.7}O_{19}$ ($x = 0.0, 0.1, 0.2, 0.3, 0.4, 0.5$).

Table 2. Parameters (ν_1) and (ν_2), molecular weight, force constant for octahedral and tetrahedral (K_o , K_t) and Bond length of $Ba_{1-x}Zr_{0.5x}Al_{0.3}Fe_{11.7}O_{19}$ nanoparticle.

Parameters	X=0.00	X=0.1	X=0.2	X=0.3	X=0.4	X=0.5
ν_1	602.64	596.42	604.75	572.76	557.54	581.72
ν_2	437.1	431.99	431.99	410.39	431.99	451.57
K_o (N/m)	140.0699 93	136.81 4107	136.81 4107	123.4744 3	136.81 4107	149.49 7406
K_t (N/m)	266.2559 99	260.78 8172	268.12 3727	240.5076 2	227.89 5398	248.09 1271
L (m)	5.795056 18	5.6205 3301	5.7071 9790	5.772196 6	5.7590 7865	5.6467 6923
Θ_D (K)	747.5730 6	739.42 679	745.41 606	706.8848 5	711.47 207	742.93 551

Fig 4 shows the tetrahedral site stretching vibrations at 602.64 cm⁻¹ in $Ba_{1-x}Zr_{0.5x}Al_{0.3}Fe_{11.7}O_{19}$ ($x = 0.0, 0.1, 0.2, 0.3, 0.4, 0.5$) M-Type ferrite, whereas the octahedral site stretching vibrations appear at 437.10 cm⁻¹. These two vibration peaks indicate the hexaferrite phase and the stretching of the Fe-O band. In other words, the hexaferrite structure is guaranteed to have molecular ($Fe^{3+}O^{2-}$) vibrations on a fundamental level due to the existence of two bands. (ν_1) is larger than (ν_2) because the tetrahedral site occupies more vibrational modes than the octahedral site due to the shorter bond length. Changes in the internuclear distance between Fe-O ions in the octahedral and tetrahedral sites are what lead to changes in band position.

The effective mass is calculated as where M_{Fe} is the iron mass and M_O is the oxygen mass[23].

$$\mu = \frac{M_{Fe} * M_O}{M_{Fe} + M_O} \quad (4)$$

The force constants K_T and K_O are determined using the tetrahedral and octahedral bands in accordance with the following relation:[24].

$$K = 4\pi^2 c^2 \nu^2 \mu \quad (5)$$

In this case, μ represents the decreased mass of the cation, " ν " denotes the vibrational frequency of the tetrahedral or octahedral arrangement, and " c " stands for the speed of light[25].

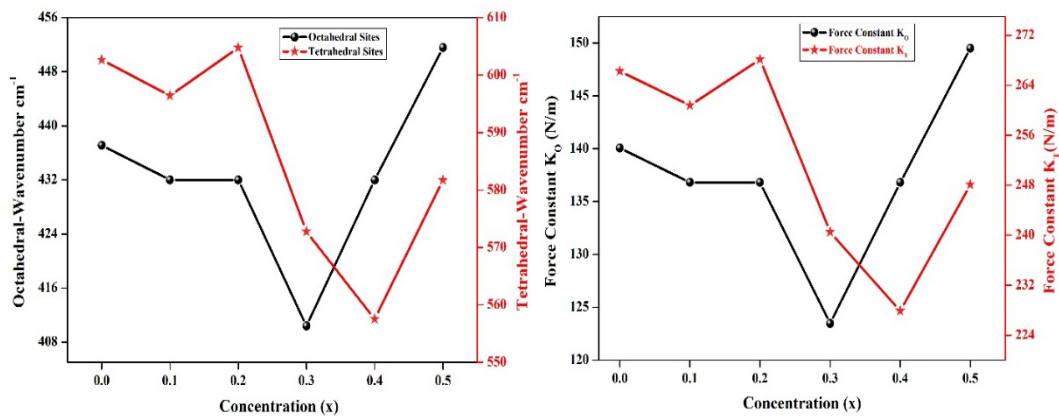


Fig. 4. (a) Variation of wave numbers at A and B sites with Zr-Al concentration. (b) force constants with Zr-Al concentration (x) at the tetrahedral and octahedral sites.

$$L = \sqrt{\left(\frac{a^2}{3} + \left(\frac{1}{2} - U\right)^2 C^2\right)} \quad (6)$$

$$U = \frac{a^2}{3C^2} + 0.25 \quad (7)$$

The tetrahedral site has a force constant between 268.123 and 227.895 Nm^{-1} , whereas the octahedral site has a force constant between 140.069 and 123.474 Nm^{-1} . Table 2 shows how the redistribution of cations across A sites is responsible for the observed change in the force constant upon Zr-Al substitution[6, 26]. Fig. 4 (a) displays the concentration-dependent variation of the wave numbers at the A and B sites, and fig 4 (b) displays the concentration(x) dependent variation of the force constants at the tetrahedral and octahedral sites. The force constant K_O and K_T are depend on the lattice parameters.

Table 2 displays the overall composition's bond length variation and its increasing trend with substitution. Zr-Al doped M-type ferrites Debye temperatures are calculated as follows[27]:

$$\theta_D = \frac{hc}{K_b} * v_{av} = 1.438 * v_{av} \quad (8)$$

where $v_{av} = (v_1 + v_2)/2$ represents the mean of the absorption bands (v_1, v_2). The value of Debye temperature is obtained from this relation suggested by the Waldron are given in the table 2. The change in Debye temperature as a function of composition is seen in Fig. θ_D falls between $x = 0$ and $x = 0.3$, before rising between $x = 0.3$ and $x=0.5$. The principle of specific heat may be used to explain this behavior. For $x \leq 0.3$, the absorption of some heat by electrons and the possible drop in θ_D indicate that the conduction in these samples is n-type. The $x > 0.3$ samples then experience a phase transition to the p-type, with a subsequent increase in θ_D due to electron-transfer heat absorption. As a result, the specific heat and, therefore, Debye's temperature should be substantially influenced by electrons[24, 28, 29].

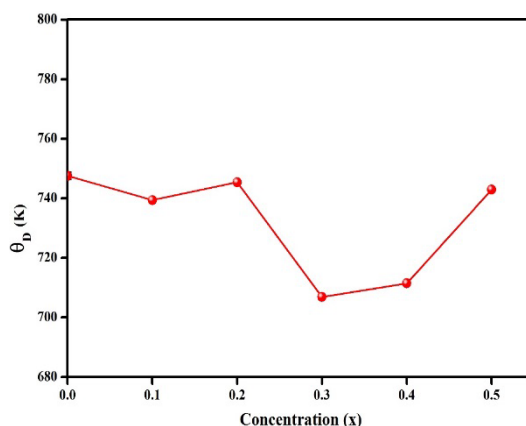


Fig. 5. The effect of Zr-Al ions concentration on the variation of the Debye temperature.

4. Conclusion

Zr-Al substituted Ba hexaferrite nanomaterials have been successfully synthesized using a low-cost sol-gel technique. For $x = 0.1$ and 0.2 , the values of M_s and M_r increase from 0.411 to 0.496 and 0.04 to 0.051 respectively after that for $x = 0.3$ to $x = 0.5$ they show decreasing trend. Moreover, with increasing the substitution level, the H_c values demonstrated increasing trend from 0.00000118 to 0.0000179. In FTIR, the existence of the bands confirms the hexagonal structure of Ba based M-type ferrites from 400-4000 cm^{-1} . The magnetic analysis suggested that the synthesized compounds may be useful as perpendicular magnetic recording medium.

Acknowledgements

The authors would like to acknowledge the Researcher's Supporting Project Number (RSP2024R269) King Saud University, Riyadh, Saudi Arabia, for their support in this work.

References

- [1] N. Yasmin, M.Z. Iqbal, M. Zahid, S.F. Gillani, M.N. Ashiq, I. Inam, S. Abdulsatar, M. Safdar, M. Mirza, *Ceramics International*, 45 (2019) 462-467; <https://doi.org/10.1016/j.ceramint.2018.09.190>
- [2] C. Singh, S.B. Narang, I. Hudiara, Y. Bai, K. Marina, *Materials Letters*, 63 (2009) 1921-1924; <https://doi.org/10.1016/j.matlet.2009.06.002>
- [3] C. Liu, X. Liu, S. Feng, K.M.U. Rehman, M. Li, C. Zhang, H. Li, X. Meng, *Journal of Magnetism and Magnetic Materials*, 436 (2017) 126-129; <https://doi.org/10.1016/j.jmmm.2017.04.040>
- [4] T. Tchouank Tekou Carol, J. Sharma, J. Mohammed, S. Kumar, A. Srivastava, *Recent Advances in Fundamental and Applied Sciences: RAFAS2016*, 1860 (2017) 020008; <https://doi.org/10.1063/1.4990307>
- [5] S. Ketov, Y.D. Yagodkin, A. Lebed, Y.V. Chernopyatova, K. Khlopkov, *Journal of Magnetism and Magnetic Materials*, 300 (2006) e479-e481; <https://doi.org/10.1016/j.jmmm.2005.10.199>
- [6] W. Abbas, I. Ahmad, M. Kanwal, G. Murtaza, I. Ali, M.A. Khan, M.N. Akhtar, M. Ahmad, *Journal of Magnetism and Magnetic Materials*, 374 (2015) 187-191; <https://doi.org/10.1016/j.jmmm.2014.08.029>
- [7] M.R. Dhondale, A.G. Nambiar, M. Singh, A.R. Mali, A.K. Agrawal, N.R. Shastri, P. Kumar, D. Kumar, *Journal of Pharmaceutical Sciences*, (2023); <https://doi.org/10.1016/j.xphs.2023.02.005>
- [8] H.A. Shahia, M.S. Shifa, Z. Mehboob, M. Hashim, F. ur Raheem, *Journal of Materials and Physical Sciences*, 2 (2021) 45-53; <https://doi.org/10.52131/jmps.2021.0201.00015>
- [9] H. Wang, D.W. Brandl, F. Le, P. Nordlander, N.J. Halas, *Nano letters*, 6 (2006) 827-832; <https://doi.org/10.1021/nl060209w>
- [10] Y. Wang, L. Li, H. Liu, H. Qiu, F. Xu, *Materials Letters*, 62 (2008) 2060-2062; <https://doi.org/10.1016/j.matlet.2007.11.026>
- [11] Z. Li, L. Chen, C. Ong, *Journal of applied physics*, 92 (2002) 3902-3907; <https://doi.org/10.1063/1.1506387>
- [12] M. Sadat, R. Patel, J. Sookoor, S.L. Bud'ko, R.C. Ewing, J. Zhang, H. Xu, Y. Wang, G.M. Pauletti, D.B. Mast, *Materials Science and Engineering: C*, 42 (2014) 52-63; <https://doi.org/10.1016/j.msec.2014.04.064>
- [13] A. Haq, M. Anis-ur-Rehman, *Physica B: Condensed Matter*, 407 (2012) 822-826; <https://doi.org/10.1016/j.physb.2011.11.038>
- [14] G.A. Ashraf, L. Zhang, W. Abbas, G. Murtaza, *Ceramics International*, 44 (2018) 18678-18685; <https://doi.org/10.1016/j.ceramint.2018.07.096>
- [15] Y. Yang, *Magnetochemistry*, 8 (2022) 118; <https://doi.org/10.3390/magnetochemistry8100118>
- [16] M.N. Ashiq, M.J. Iqbal, M. Najam-ul-Haq, P.H. Gomez, A.M. Qureshi, *Journal of magnetism and magnetic materials*, 324 (2012) 15-19; <https://doi.org/10.1016/j.jmmm.2011.07.016>
- [17] Y. Slimani, N. Algarou, M. Almessiere, A. Sadaqat, M. Vakhitov, D. Klygach, D. Tishkevich, A. Trukhanov, S. Güner, A. Hakeem, *Arabian Journal of Chemistry*, 14 (2021) 102992; <https://doi.org/10.1016/j.arabjc.2021.102992>
- [18] A. Majeed, M.A. Khan, R. Ahmad, M.Y. Lodhi, I. Ahmad, *Solid State Sciences*, 100 (2020) 106090; <https://doi.org/10.1016/j.solidstatesciences.2019.106090>
- [19] J. Xu, H. Zou, H. Li, G. Li, S. Gan, G. Hong, *Journal of Alloys and Compounds*, 490 (2010)

- 552-556; <https://doi.org/10.1016/j.jallcom.2009.10.079>
- [20] J. Singh, C. Singh, D. Kaur, H. Zaki, I. Abdel-Latif, S.B. Narang, R. Jotania, S.R. Mishra, R. Joshi, P. Dhruv, *Journal of Alloys and Compounds*, 695 (2017) 1112-1121; <https://doi.org/10.1016/j.jallcom.2016.10.237>
- [21] A. Alsmadi, I. Bsoul, S. Mahmood, G. Alnawashi, F. Al-Dweri, Y. Maswadeh, U. Welp, *Journal of Alloys and Compounds*, 648 (2015) 419-427; <https://doi.org/10.1016/j.jallcom.2015.06.274>
- [22] M.A. Almessiere, Y. Slimani, M. Sertkol, M. Nawaz, A. Baykal, I. Ercan, *Results in Physics*, 13 (2019) 102244; <https://doi.org/10.1016/j.rinp.2019.102244>
- [23] M. Suthar, P. Roy, *Materials Science and Engineering: B*, 283 (2022) 115801; <https://doi.org/10.1016/j.mseb.2022.115801>
- [24] M. Hashim, N. Boda, A. Ahmed, S. Sharma, D. Ravinder, E. Sumalatha, A. Ul-Hamid, M.M. Ismail, M. Chaman, S.E. Shirsath, *Applied Physics A*, 127 (2021) 526; <https://doi.org/10.1007/s00339-021-04686-4>
- [25] A. Sahai, N. Goswami, *Physica E: Low-dimensional Systems and Nanostructures*, 58 (2014) 130-137; <https://doi.org/10.1016/j.physe.2013.12.009>
- [26] K.A. Kumar, R. Bhowmik, *Materials Chemistry and Physics*, 146 (2014) 159-169; <https://doi.org/10.1016/j.matchemphys.2014.03.015>
- [27] R. Kadam, R. Borade, M. Mane, D. Mane, K. Batoo, S.E. Shirsath, *RSC advances*, 10 (2020) 27911-27922; <https://doi.org/10.1039/D0RA05274D>
- [28] S. Mazen, S. Mansour, E. Dhahri, H. Zaki, T. Elmosalami, *Journal of Alloys and Compounds*, 470 (2009) 294-300; <https://doi.org/10.1016/j.jallcom.2008.02.035>
- [29] M. Beyranvand, A. Gholizadeh, *Journal of Materials Science: Materials in Electronics*, 31 (2020) 5124-5140; <https://doi.org/10.1007/s10854-020-03073-8>